THE JOURNAL OF PHYSICAL CHEMISTRY Letters

Letter

pubs.acs.org/JPCL

# Discerning Variable Extents of Interdomain Orientational and Structural Heterogeneity in Solution-Cast Polycrystalline Organic Semiconducting Thin Films

Cathy Y. Wong,[†] Brendan D. Folie,[‡] Benjamin L. Cotts,[†] and Naomi S. Ginsberg*[,†,‡,§,∥,⊥]

[†]Department of Chemistry and [‡]Department of Physics, University of California, Berkeley, California 94720, United States

[§]Physical Biosciences and [∥]Materials Sciences Division, Lawrence Berkeley National Laboratory, Berkeley, California 94720, United States

[⊥]Kavli Energy NanoSciences Institute, Berkeley, California 94720, United States

Supporting Information

**ABSTRACT:** By spatially resolving the polarized ultrafast optical transient absorption within several tens of individual domains in solution-processed polycrystalline small-molecule organic semiconducting films, we infer the domains' extents of structural and orientational heterogeneity. As metrics, we observe variations in the time scales of ultrafast excited state dynamics and in the relative strength of competing resonant probe transitions. We find that films of 2,8-difluoro-5,11-bis(triethylsilylethynyl)anthradithiophene (diF-TES-ADT) exhibit a much higher degree of both structural and orientational heterogeneity among their domains than do films of 6,13-bis(triisopropylsilylethynyl)pentacene (TIPS-Pn), despite the apparent structural similarity between these two small molecules. Since both molecules feature prominently in solution-processed organic transistors, correlating the extent of heterogeneity to bulk transport using our approach will be highly valuable toward determining the underlying design principles for creating high-performing devices. Furthermore, our ability to characterize such variation in heterogeneity will enable fundamental studies of the interplay between molecular dynamics and driving forces in controlling emergent unequilibrated structures.

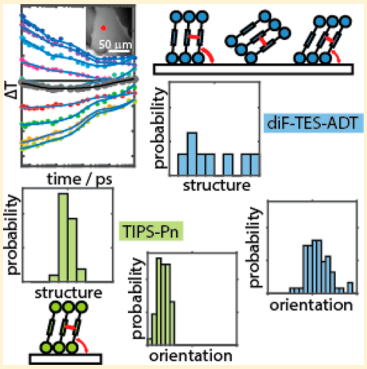


Small-molecule organic semiconducting thin films serve many applications in solution-processed electronics. In many cases, they form polycrystalline films with a wide range in the size and shape of individual domains. The high degree of intermolecular order in these films predisposes them to applications in solution-processed transistors, where comparatively high charge carrier mobilities can be engineered due to regular $\pi$-stacking or other forms of orbital overlap along a particular in-plane direction.[1,2] Understanding how the crystalline intermolecular packing in these materials determines their electronic properties is of paramount importance in explaining bulk transport metrics such as charge carrier mobilities. Yet, the variation in structure and orientation exhibited among crystalline domains also contributes to these bulk metrics, and is generally averaged out in measurements of structure, electronic structure, optical properties and excited state dynamics. Being able to determine the differences between an average structure's electronic properties and between the effect of structural heterogeneity on overall film properties is important in order to determine the root cause of limitations to transport properties and in order to further improve them.

Ultrafast spectroscopies, such as transient absorption (TA),[3−5] have provided detailed information about the electronic structure and dynamics of photoexcitable organic semiconducting materials.[6−8] The ultrafast excited state dynamics of electronically coupled materials are extremely sensitive to small variations in the Coulomb interactions between coupled molecules that arise due to their particular spatial configurations.[1,9−11] Although such measurements are generally performed in bulk with laser pulse waists exceeding the size of individual crystalline domains, transient absorption microscopy (TAM) has recently been used to study these thin films[12,13] in addition to other structures with heterogeneous electronic and transport properties.[14−21] Beyond the obvious advantage of no longer averaging over the optical signatures of multiple crystalline domains, there is a further incentive to collecting very small signals from focal volumes orders of magnitude smaller than is typically done with TA. Because the individual molecular constituents in these polycrystalline films are often planar, the crystals formed are generally very anisotropic. By virtue of measuring individual crystallites, single-domain TAM can therefore additionally utilize the strong light polarization response of these individual domains in order to more precisely determine the material's excited state dynamic time scales that are extracted from ultrafast measure-

**Received:** July 5, 2015
**Accepted:** July 30, 2015

  

DOI: 10.1021/acs.jpclett.5b01416
*J. Phys. Chem. Lett.* 2015, 6, 3155−3162

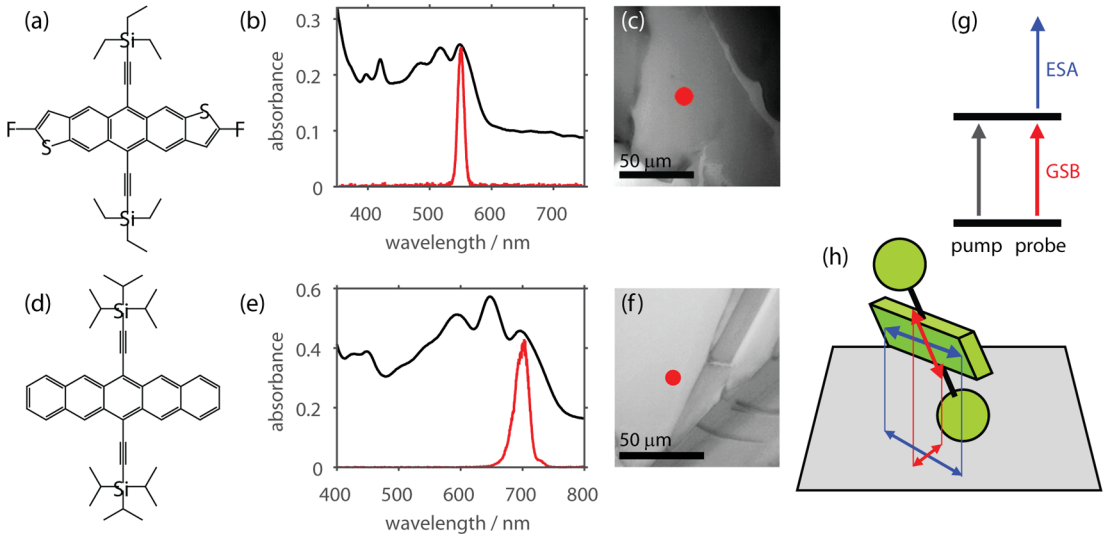


**Figure 1.** (a) Chemical structure of diF-TES-ADT, (b) linear absorption spectrum of diF-TES-ADT film (black), and laser spectrum (red), and (c) linear transmission image of a diF-TESADT film; spot indicates laser spot size. (d) Chemical structure of TIPS-Pn, (e) linear absorption spectrum of TIPS-Pn film, and laser spectrum, and (f) linear transmission image of a TIPS-Pn film; spot indicates laser spot size. (g) Schematic energy levels and transitions induced by pump and probe pulses. (h) Cartoon of a single molecule at a typical orientation with respect to substrate. Rectangular prism represents aromatic core, spheres represent bulky side groups. Arrows represent ground state bleach (red) and excited state absorption (blue) transition dipole moments and their projections on to the substrate plane.

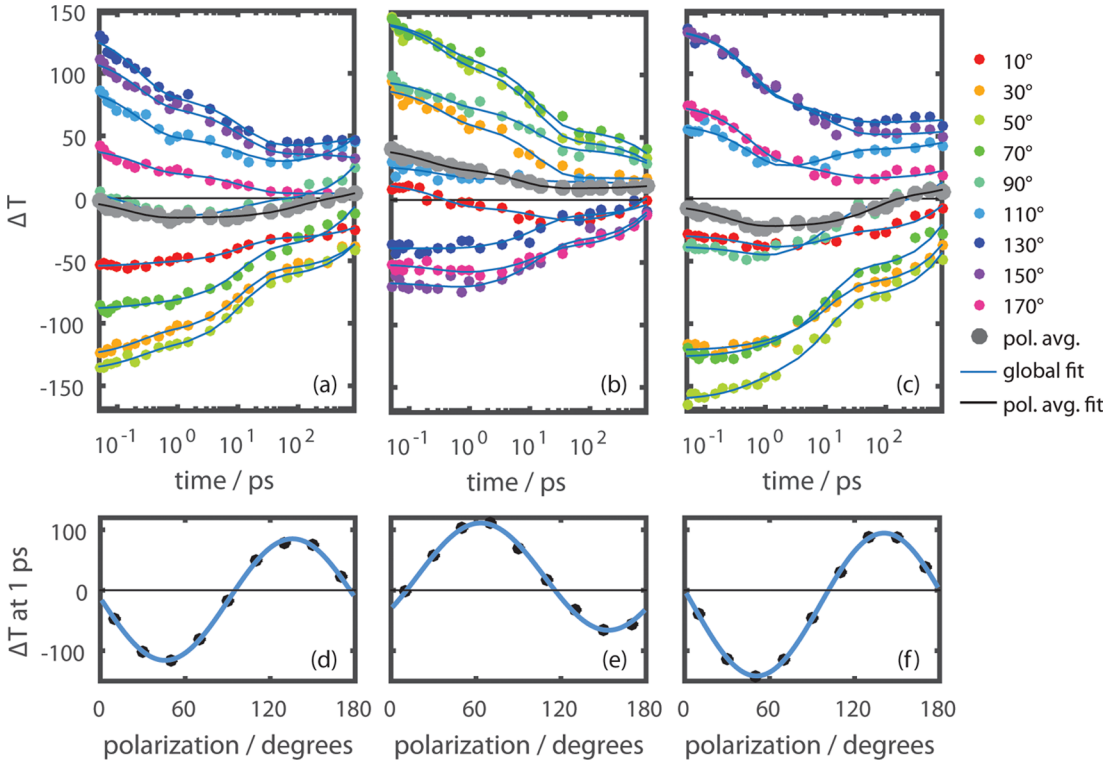


**Figure 2.** (a–c) Transients collected using various probe polarizations in individual diF-TES-ADT domains, along with global triexponential fits (blue). Signal can also be averaged over all polarizations (gray) and fit (black), which should be analogous to a bulk measurement if all domains were orientationally and structurally identical to the domain studied. (d–f) Dependence of TA signal on probe polarization at pump–probe delay time of 1 ps. Blue lines are fits to a cosine squared function.

ments.[12] Although it has not been previously demonstrated, obtaining transient information on the single-domain level should, in principle, enable a direct comparison of electronic structure and dynamics among the domains in a film. Such a comparison should reveal the degree of interdomain heterogeneity in much the same way as single-molecule measurements have done for solution-phase studies or for impurities in solid matrices.[22−24]

In previous work we illustrated the utility of polarized TAM for uncovering rotations about the substrate normal in otherwise structurally similar domains of small-molecule solution-processed organic semiconducting films.[12] Here we



DOI: 10.1021/acs.jpclett.5b01416
J. Phys. Chem. Lett. 2015, 6, 3155−3162

obtain the polarized TA of individual domains of 2,8-difluoro-5,11-bis(triethylsilylethynyl)anthradithiophene (diF-TES-ADT)[25−30] films and uncover for the first time heterogeneity in both electronic structure and nonazimuthal orientation of the domains in this type of organic polycrystalline film. We quantify these interdomain heterogeneities, respectively, based on variations in excited state dynamics time scales and based on variations in the relative strength of two resonant probe transitions. Performing a similar analysis on the single-domain TA that we previously obtained[12] for films of the structurally similar 6,13-bis(triisopropylsilylethynyl)pentacene (TIPS-Pn)[1,6,31−36] molecule reveals significantly less interdomain heterogeneity. The variations observed in diF-TES-ADT films indicate that measuring TA with spatial resolution can be essential to accurately characterize organic semiconducting film excited states and their dynamics, the relationship of these excited states to film structure, and the variability within a film. The varying degree of heterogeneity surmised in contrasting the diF-TES-ADT and TIPS-Pn films furthermore indicates that the combined choice of molecules and their respective casting conditions, however similar, leads to very different extents of interdomain heterogeneity, a parameter that could be important in determining charge transport over larger scales. Our newfound ability to sensitively characterize and quantify structural and orientation variability among domains in solution-processed polycrystalline films therefore provides a sought after avenue for explaining which types of microscopic heterogeneities dominate the resulting macroscopic transport.

TAM measurements were performed within individual domains in a dropcast thin film of diF-TES-ADT and were compared to analogous measurements in dropcast thin films of TIPS-Pn. Figure 1c,f show representative transmission images of the two different types of films. The colored spots in these images represent the approximate laser spot sizes used for the TAM measurements. Since the measurement volumes are smaller than the size of the domains, the resulting transient absorption signal is caused by the excitations generated in only one domain. Although diF-TES-ADT and TIPS-Pn have similar molecular structures (Figure 1a,d), packing structures, and linear absorption spectral shapes (Figure 1b,e), we find that their excited state dynamics differ. Figure 2a−c reports examples of the TA measured at the band edge in diF-TES-ADT films using various probe polarizations. Figure 2d−f shows the corresponding dependence of the TA signals on the probe light pulse polarization at a pump−probe delay time of 1 ps. We reported similarly obtained TA within TIPS-Pn domains in refs 12 and 13, some other examples of which are presented in Supporting Information Figure S1 and Table S1.

To explain and analyze the features of the data in Figure 2, we first describe the transitions accessible to the probe light pulse and their couplings to the pulse's polarized electric field. The clear polarization dependence of the TA signals indicates that the examined areas have anisotropic structure. The signal can be either positive or negative, depending on the probe polarization. This indicates that, after photoexcitation, the probe is resonant with both excited state absorption (ESA) and ground state bleach (GSB) transitions, which result in negative and positive transient absorption signals, respectively (Figure 1g). These transitions must have transition dipole moments that have different orientations in the lab-frame, so the coupling of the probe to each of these transitions will change with the probe polarization (Figure 1h) for a given domain. In comparing different domains for a given probe polarization, domains oriented so that their GSB transition (typically along the polyacene short axis) is aligned with the probe field will have dominantly positive TA signals as compared with those domains oriented so that their ESA transitions (typically along the polyacene long axis) align with the field. The molecules studied in this work have packing structures with a single molecule per unit cell, so the delocalized crystal transition dipole moments point in the same directions as those of an individual molecule (Figure 1h). In the diF-TES-ADT domain measured in Figure 2a,d, about half of the probe polarizations produce positive signals, which means that GSB dominates ESA, and half of the probe polarizations produce negative signals, where ESA instead dominates GSB. The projection of these two different transition dipole moments onto the sample plane determines their relative abilities to couple to the probe pulse's polarized electric field. The relative amounts of GSB and ESA can thus be used to characterize and compare the nonazimuthal orientation of different crystalline domains in a film. We return to domain orientation after first exploring attributes of the single-domain polarized TA that reveal structural heterogeneity.

The spatial resolution of TAM allows for the comparison of dynamics in individual domains in order to infer structural variations among them. Transients can be collected at a number of different probe polarizations. Because the pump polarization remains the same for all measurements in a particular domain, the initial exciton population is the same for each measurement in the polarization series; the differences among the polarized transients in a given domain are due to the polarization-dependent coupling strength between the probe and the available transitions. The physical processes which occur to the photogenerated exciton population depend on the electronic structure and dynamics of the domain, and will be the same irrespective of the probe polarization. Thus, in fitting the data to a weighted sum of exponential decays, the time constants in the transients collected at each probe polarization should be the same, but the amplitudes should change owing to the coupling between the probe and the available transitions. With this in mind, a global fit was performed using the collection of transients at all probe polarizations for each individual domain. The transient for each probe polarization was fit to the function $y = A_1 \exp(-x/t_1) + A_2 \exp(-x/t_2) + A_3 \exp(-x/2300\ \text{ps}) + c$. In the fit to $y$, the time constants $t_1$ and $t_2$ are global, while the pre-exponential amplitudes, $A_1$, $A_2$, and $A_3$, and offset, $c$, are different for each polarization. The time constant of the third exponential was set to the fluorescence lifetime of diF-TES-ADT, which represents the longest time scale of loss of the singlet excited state population, and which has been measured in films to be 2300 ps.[37] The resulting fits are shown as blue curves in Figure 2a−c, with extracted time constants shown in Table 1. The fit $A_1$, $A_2$, $A_3$, and $c$ values, along with plots of the dependence of these fit values on probe polarization, can be found in Supporting Information Table S2, along with similar fitting on single-domain TA of TIPS-Pn films (Supporting Information Figure S1 and Tables S1 and S3). The amplitudes have a cosine-squared dependence on polarization, as would be expected from the varying coupling of the probe pulse electric field vector to the transition dipole moments (Supporting Information Figure S2).

The time constants from the global fit to the diF-TES-ADT polarized transients can be compared to the fit of the average of the signal at each probe polarization, shown as the gray data points in Figure 2a−c. This polarization average would be



DOI: 10.1021/acs.jpclett.5b01416
J. Phys. Chem. Lett. 2015, 6, 3155−3162

**Table 1. Time Constants from Fits for Three Different diF-TES-ADT Domains**[a]

| | global | | polarization averaged | |
|---|---|---|---|---|
| domain | $t_1$/ps | $t_2$/ps | $t_1$/ps | $t_2$/ps |
| (a) | 0.23 ± 0.02 | 12.1 ± 0.8 | 0.16 ± 0.04 | 90 ± 34 |
| (b) | 0.33 ± 0.05 | 13.5 ± 1.1 | 0.21 ± 0.05 | 7.1 ± 1.4 |
| (c) | 0.60 ± 0.06 | 11.4 ± 0.9 | 0.24 ± 0.08 | 67 ± 19 |

[a]TA signal was fit to $y = A_1 \exp(-x/t_1) + A_2 \exp(-x/t_2) + A_3 \exp(-x/2300\ \text{ps}) + c$, where $t_1$ and $t_2$ are global when data collected at all probe polarizations are used. $1-\sigma$ confidence intervals are shown. Tables and plots of $A_1$, $A_2$, $A_3$, and $c$ are provided in the Supporting Information.

analogous to a bulk measurement, provided that each of the domains in the sample were identical both in structure and nonazimuthal orientation. Yet, the differences among the time constants of the three polarization-averaged fits demonstrate that even averaging over rotations in the substrate plane is insufficient to reach the homogenized transient obtained for a bulk measurement. These differences therefore report on the heterogeneity of the domains in the film. By contrast, similarly obtained polarization-averaged transients in TIPS-Pn domains consistently produce similar sets of time constants (Supporting Information Table S1 and refs 12 and 13). The diF-TES-ADT polarization-averaged data were fit to the same triexponential function as the polarized TAM traces, and the resulting time constants are also reported in Table 1. The differences in the time constants resulting from fits to the averaged data and from the global fits to the polarization dependent series of data show that the dynamics can be much more accurately determined by using TAM to measure individual domains with multiple probe polarizations. Furthermore, the fits to the averaged data generally have more uncertainty, as indicated in Table 1, likely because of the mutual cancellation of ESA and GSB upon averaging. In particular, the intermediate time constant $t_2$ is substantially lengthened from ~10 ps to several tens of picoseconds when averaging over polarizations, and the error in the parameter value increases commensurately. In bulk measurements (Supporting Information Figure S3 and Table S4), which especially suffer from the cancellation of ESA and GSB, this time constant is even more difficult to define, obscuring the true dynamics that occur in each domain. This is not surprising, as compared to bulk measurements or to a single polarization-averaged transient, the set of single domain polarized transient data introduces far more fitting constraints than additional fit parameters. The difference between the number of constraints and the number of parameters scales as the number of probe polarizations employed multiplied by the difference between the number of time points measured (23) and the number of free parameters (4) per polarization employed.

As shown in Table 1, the three diF-TES-ADT domains studied in Figure 2 have similar dynamics, in that there are fast (sub-picoseconds), intermediate (tens of picoseconds), and long (~2300 ps) time scale processes observed in each one. The time constants extracted from global fits for the three different domains do not, however, agree with one another to within $1-\sigma$ confidence intervals. Full transients, similar to those shown in Figure 2a–c, were collected for 8 different diF-TES-ADT domains, and their time constants were determined by global fits, as described above. Figure 3a,b shows histograms of all of these $t_1$ and $t_2$ values, respectively. The $t_1$ and $t_2$ values are reported as fractions of the average values from these eight

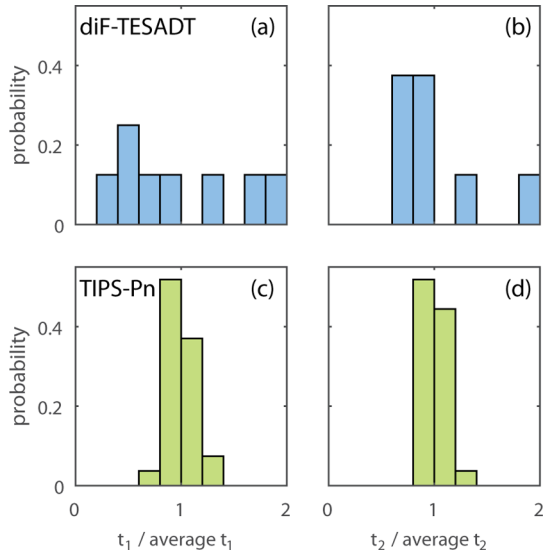


**Figure 3.** Histograms of time constants $t_1$ (a,c) and $t_2$ (b,d) from global fits of TA signal collected from individual domains of diF-TES-ADT (a,b) and neat TIPS-Pn (c,d). Time constants are reported as fractions of their average values.

domains, 0.595 and 15.9 ps, respectively. This can be compared to Figure 3c,d, which shows histograms of the fast and intermediate time constants obtained from the global fits of transients collected for 27 different TIPS-Pn domains. The average $t_1$ and $t_2$ values for these domains are 0.046 and 3.17 ps. The percentage variability in time constants observed in diF-TES-ADT is several times that observed in TIPS-Pn films, especially apparent for $t_1$. The spread of $t_1$ and $t_2$ values from eight domains of diF-TES-ADT is larger than the spread of values found after 27 measurements of TIPS-Pn.

We note briefly that we have also performed simultaneous fits of the diF-TES-ADT polarized TAM traces to a kinetic model, similar to that described for TIPS-Pn in ref 12. The excellent fits to all data in Figure 2 are shown in Supporting Information Figure S4, Tables S5 and S6, and accompanying text, and imply that the three time scales that we observe are consistent with singlet vibrational relaxation, singlet fission,[7,38−41] and fluorescence decay. Variations that we observe in the short and intermediate excited state dynamics time scales among the domains of diF-TES-ADT films could be due to small variations in lattice constants that respectively alter the lattice vibrational modes and the singlet−triplet energy gap.

Before discussing the relationship between variations in time constants and variations in domain structure, we conclude our presentation of results by pointing out the relative extent of GSB and ESA among domains, as an indicator of interdomain heterogeneity in nonazimuthal orientation. Inspection of the data in Figure 2 also shows that the relative extent of GSB and ESA can vary among domains of diF-TES-ADT. For example, GSB dominates over a larger range of probe polarizations in the domain measured in Figure 2b,e, while ESA dominates over a larger polarization range in the domain measured in Figure 2c,f. In order to determine a metric for the relative strength of GSB and ESA, the TA signal at a pump−probe delay time of 1 ps as a function of probe polarization is fit to a cosine-squared function that oscillates both above and below zero (curves in Figure 2d–f). This oscillation's offset from zero indicates the GSB strength relative to the ESA strength. The offset of the curve, normalized to its peak-to-peak amplitude, shows which


DOI: 10.1021/acs.jpclett.5b01416
J. Phys. Chem. Lett. 2015, 6, 3155−3162

transition dominates in a given domain when the excitation light is incident normal to the substrate. For the domains represented in Figure 2c,d,e, these offset parameters are −0.08, 0.18, and −0.03, respectively. This indicates that ESA dominates over GSB in the domains of Figure 2c,e, while GSB dominates over ESA in the domain of Figure 2d.

The nonazimuthal orientational heterogeneity of crystalline domains within a sample can be visualized by constructing histograms of this offset parameter value collected in different domains. Using TAM, 62 diF-TES-ADT domains were inspected, and their offset parameters calculated. The histogram of the resulting normalized offsets, shown in Figure 4a,

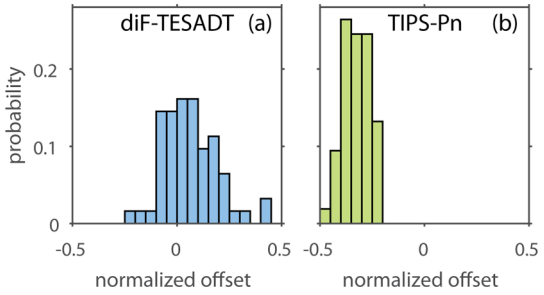


**Figure 4.** Histograms of normalized offsets in single domains within thin films of (a) diF-TES-ADT and (b) TIPS-Pn. Bin size is 0.05.

indicates that the offset parameter in the inspected domains can range from −0.22 to +0.42. These domains show more heterogeneity in their offset parameters than those of TIPS-Pn: Figure 4b shows a histogram of the offset parameters measured for 51 domains of TIPS-Pn, centered more narrowly about ca. −0.35. The distribution of offset parameters in the measured TIPS-Pn domains is more than 2 times narrower than the measured diF-TES-ADT domain distribution.

Before discussing our results, we note that the combination of subdomain optical resolution and the resulting polarization sensitivity of our measurements has been essential to form our observations and carry out the above analysis. Bulk TA measurements average over orientational and structural variations among domains and suffer—especially in diF-TES-ADT—from the cancellation of competing polarization-dependent TA contributions in a spatial average, therefore obfuscating the true excited state dynamics that aid in comparing structures (Supporting Information Figure S3). Although spatially resolved linear absorption measurements[42,43] might be sensitive enough to decode variations in nonazimuthal orientation, they are not capable of discerning small differences in crystal structure. While X-ray diffraction is often used to obtain crystal structures, and even various polymorphs, the spatial resolution of the diffractive measurements does not generally enable single domain resolution, nor does it enable a direct connection to electronic structure or dynamics.[29,44−46]

Having observed single-domain polarized TA in both diF-TES-ADT and TIPS-Pn and having developed metrics to statistically analyze variations among TA features of domains, we now physically interpret and discuss the implications of our analysis. We distinguish between the structural variations inferred from variations in transient time constants, illustrated in Figure 3 and discussed next, and the primarily orientational variations inferred from variations in the offset parameter, illustrated in Figure 4 and discussed thereafter.

Heterogeneity in dynamics is indicative of structural disorder among crystalline domains. Namely, differences in the crystal lattice parameters should generate differences in intermolecular electronic coupling and in the resulting electronic structures of the crystalline domains, some examples of which are sketched in Figure 5a,b. Our measurements are sensitive to these differences through the statistically significant variations that we observe in the transient time constants for diF-TES-ADT (Figure 3a,b). We note that, despite the sensitivity of our measurements, we observe no similarly sized variation among TIPS-Pn domains (Figure 3c,d). We thus conclude that the casting of our diF-TES-ADT film supported the nucleation of slightly different crystal structures (Figure 5a), whereas those in the TIPS-Pn films seem far more homogeneous (Figure 5b). Films of diF-TES-ADT are known to exhibit two polymorphs, with a transition temperature near room-temperature.[28] It is therefore possible that both crystal forms exist in our films, although the distribution of structural parameters that we have obtained is not obviously bimodal. While it is beyond the scope of this work, this possibility could be verified with X-ray diffraction. It is possible that the heterogeneity of crystal structures we infer in diF-TES-ADT films causes the singlet−triplet energy gap to fluctuate, resulting in variable rates of singlet fission among domains.

Heterogeneity in the offset parameter is indicative of nonazimuthal orientational disorder. Here, we distinguish between rotations of the crystal structure about the normal to the substrate plane and all other rotations. The former do not affect the offset parameter since the projections of the GSB and ESA transition dipole moments relative to one another (Figure 1h) are preserved upon rotation about the normal. On the other hand, all other rotations of a crystallite (Figure 5c) do not preserve the relative strength of these projections and are hence able to alter the offset parameter. (Although differences in packing structure could also, in principle, affect this parameter by altering the electronic structure, we assume that they are a less significant contribution.) In TIPS-Pn films, there are hardly any variations in the offset parameter (Figure 4b,c). Therefore, we interpret that the angle of the TIPS-Pn molecules with respect to the substrate is essentially preserved in all of the many measured domains (Figure 5b). By contrast,

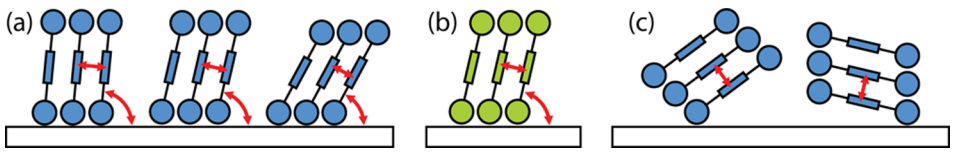


**Figure 5.** Schematic illustration of possible variations in structure and nonazimuthal orientation of small molecule crystal domains. (a) Structural variations, as inferred for diF-TES-ADT, involve changing the intermolecular spacing and angle with respect to the substrate. (b) TIPS-Pn appears to maintain a ∼single intermolecular spacing and angle with respect to the substrate. (c) The nonazimuthal orientation of diF-TES-ADT crystal grains appears to be variable even if independent of lattice spacing.



DOI: 10.1021/acs.jpclett.5b01416
J. Phys. Chem. Lett. 2015, 6, 3155−3162

it appears that the diF-TES-ADT crystal grains can take on various orientations rotated about an axis in the substrate plane (Figure 5c), as evidenced by the much larger spread in offset parameters observed over many diF-TES-ADT domains (Figure 4a). Although it is possible that there exists a positive correlation between the extent of structural and orientational variations in small-molecule organic semiconducting films, a specific form of interdependence in our time constant and GSB/ESA metrics is not obvious.

In the two types of small-molecule films that we have studied, we observe striking differences in the extent of structural and orientational variations. In the context of organic thin film transistors, a film's degree of interdomain heterogeneity could correlate to its macroscopic mobility, and this degree of heterogeneity could determine device consistency. For solution-cast polycrystalline films with impressive intradomain mobilities along the $\pi$-stacking direction, charge transport isotropy is important for device consistency.[47,48] For example, a randomized array of crystallites provides a higher multiplicity of charge carrier scattering trajectories from source to drain than a single crystal whose $\pi$-stacking direction is misaligned with the channel. It is possible that the interdomain orientational heterogeneity that we discovered promotes such charge transport isotropy and could be used as a predictor for consistent, high-performing devices. By the same token, too much structural heterogeneity could create energetic traps. Therefore, calibrating the extent of these variations to macroscopic metrics could help to dictate the film microstructures and casting conditions that optimize overall transport in polycrystalline materials.

In sum, we have illustrated how structural and orientational heterogeneities among domains in polycrystalline small-molecule organic semiconducting films can be highly variable, even within a particular class of small molecules. To do so, it was essential to achieve single-domain specificity in performing polarized TAM on our diF-TES-ADT and TIPS-Pn thin films. The anisotropy of the crystalline domains enables the probe pulse field polarization to aid in characterizing excited state dynamics far more accurately than bulk measurements, which we used to uncover interdomain variations in crystal structure and orientation. This powerful new approach to characterizing and quantifying these interdomain variations stands to identify an important hidden variable in the quality and consistency of electronic devices. In the realm of small-molecule semiconducting films, TAM studies as a function of molecular structure, solvent, and casting conditions should establish specifically how the extent of interdomain order relates to bulk charge transport or even to multiexciton-generating efficiencies. Such patterns may furthermore enable predictive design of the most promising small molecules for switching or photovoltaic applications in solution-processed organic electronics. More generally, our approach will aid in answering the question of how to control solution-based, selective self-assembly of complex structures. The heterogeneity that we observe in kinetically trapped solids should both infer the dynamics of formation and infer the resulting structure's energy landscape to support a variety of complex functions.

## EXPERIMENTAL METHODS

*Film Preparation*. Films were created from 5 mg/mL solutions of diF-TES-ADT in toluene. For each film, ~ 150 $\mu$L of solution was dropcast onto a clean glass coverslip and then covered with a large Petri dish to slow the evaporation rate while it dried at room temperature. Likewise, an additional portion of ~150 $\mu$L of pure toluene was placed under the same Petri dish on a separate coverslip to further control the solvent vapor pressure of the casting environment. (See Supporting Information for TIPS-Pn film preparation.)

*Transient Absorption Microscopy*. TA microscopy measurements were conducted in a home-built optical microscope.[12] Briefly, 5 kHz, 550 nm center-wavelength laser pulses were used to pump the $S_0 \rightarrow S_1$ transition of diF-TES-ADT (Figure 1b). The beam was split into degenerate pump and probe pulses in a 4:1 intensity ratio and focused on the sample using a 0.4 NA objective to yield full-width half-maximum (fwhm) spot sizes between 4 and 13 $\mu$m and pulse durations of ~40 fs. A variety of pump energy fluences were employed (940 $\mu J/cm^2$ to 120 $\mu J/cm^2$), all within the linear range. Probe polarizations were varied by rotating a motorized waveplate. After passing through a single domain in the sample, the transmitted beams were collected using a second, identical objective, and the pump beam was removed via spatial filtering. The probe signal was focused onto a photomultiplier tube (PMT). The output from the PMT was coupled to a lock-in amplifier, locked to the pump chopping frequency (500 Hz) to collect the unnormalized TA signal, $\Delta T$.

## ASSOCIATED CONTENT

### Supporting Information

The Supporting Information contains polarized TAM data, fits, and fit parameters for TIPS-Pn films, bulk TA, fits, and fit parameters at multiple probe wavelengths for diF-TES-ADT films, and a kinetic model and fits of polarized TAM data for diF-TES-ADT films. The Supporting Information is available free of charge on the ACS Publications website at DOI: 10.1021/acs.jpclett.5b01416.

(PDF)

## AUTHOR INFORMATION

### Corresponding Author

*E-mail address: nsginsberg@berkeley.edu.

### Notes

The authors declare no competing financial interest.

## ACKNOWLEDGMENTS

This work has been supported by the Defense Advanced Research Projects Agency Young Faculty Award number N66001-12-1-4228 and by a David and Lucile Packard Foundation Fellowship for Science and Engineering to N.S.G. C.Y.W. thanks the Natural Sciences and Engineering Research Council, Canada for a Postdoctoral Fellowship, B.D.F. and B.L.C. each acknowledge a National Science Foundation Graduate Research Fellowship (DGE 1106400), and N.S.G. acknowledges an Alfred P. Sloan Research Fellowship.

## REFERENCES

(1) Giri, G.; Verploegen, E.; Mannsfeld, S. C. B.; Atahan-Evrenk, S.; Kim, D. H.; Lee, S. Y.; Becerril, H. A.; Aspuru-Guzik, A.; Toney, M. F.; Bao, Z. Tuning Charge Transport in Solution-Sheared Organic Semiconductors Using Lattice Strain. *Nature* **2011**, *480*, 504−508.

(2) Anthony, J. E. Functionalized Acenes and Heteroacenes for Organic Electronics. *Chem. Rev.* **2006**, *106*, 5028−5048.

(3) Lanzani, G. Pump Probe and Other Modulation Techniques. In *The Photophysics behind Photovoltaics and Photonics*; Wiley-VCH Verlag GmbH & Co. KGaA: Weinheim, Germany, 2012; p 177.



DOI: 10.1021/acs.jpclett.5b01416
J. Phys. Chem. Lett. 2015, 6, 3155−3162

(4) Megerle, U.; Pugliesi, I.; Schriever, C.; Sailer, C. F.; Riedle, E. Sub-50 Fs Broadband Absorption Spectroscopy with Tunable Excitation: Putting the Analysis of Ultrafast Molecular Dynamics on Solid Ground. *Appl. Phys. B: Lasers Opt.* **2009**, *96*, 215−231.
(5) Pollard, W. T.; Mathies, R. A. Analysis of Femtosecond Dynamic Absorption Spectra of Nonstationary States. *Annu. Rev. Phys. Chem.* **1992**, *43*, 497−523.
(6) Ramanan, C.; Smeigh, A. L.; Anthony, J. E.; Marks, T. J.; Wasielewski, M. R. Competition between Singlet Fission and Charge Separation in Solution-Processed Blend Films of 6,13-Bis-(triisopropylsilylethynyl)pentacene with Sterically-Encumbered Perylene-3,4:9,10-Bis(dicarboximide)s. *J. Am. Chem. Soc.* **2012**, *134*, 386−397.
(7) Eaton, S. W.; Shoer, L. E.; Karlen, S. D.; Dyar, S. M.; Margulies, E. A.; Veldkamp, B. S.; Ramanan, C.; Hartzler, D. A.; Savikhin, S.; Marks, T. J.; et al. Singlet Exciton Fission in Polycrystalline Thin Films of a Slip-Stacked Perylenediimide. *J. Am. Chem. Soc.* **2013**, *135*, 14701−14712.
(8) Wilson, M. W. B.; Rao, A.; Clark, J.; Kumar, R. S. S.; Brida, D.; Cerullo, G.; Friend, R. H. Ultrafast Dynamics of Exciton Fission in Polycrystalline Pentacene. *J. Am. Chem. Soc.* **2011**, *133*, 11830−11833.
(9) Lim, S.-H.; Bjorklund, T. G.; Spano, F. C.; Bardeen, C. J. Exciton Delocalization and Superradiance in Tetracene Thin Films and Nanoaggregates. *Phys. Rev. Lett.* **2004**, *92*, 107402.
(10) Troisi, A.; Orlandi, G.; Anthony, J. E. Electronic Interactions and Thermal Disorder in Molecular Crystals Containing Cofacial Pentacene Units. *Chem. Mater.* **2005**, *17*, 5024−5031.
(11) Ryno, S. M.; Risko, C.; Brédas, J.-L. Impact of Molecular Packing on Electronic Polarization in Organic Crystals: The Case of Pentacene vs TIPS-Pentacene. *J. Am. Chem. Soc.* **2014**, *136*, 6421−6427.
(12) Wong, C. Y.; Penwell, S. B.; Cotts, B. L.; Noriega, R.; Wu, H.; Ginsberg, N. S. Revealing Exciton Dynamics in a Small-Molecule Organic Semiconducting Film with Subdomain Transient Absorption Microscopy. *J. Phys. Chem. C* **2013**, *117*, 22111−22122.
(13) Wong, C. Y.; Cotts, B. L.; Wu, H.; Ginsberg, N. S. Exciton Dynamics Reveal Aggregates with Intermolecular Order at Hidden Interfaces in Solution-Cast Organic Semiconducting Films. *Nat. Commun.* **2015**, *6*, 5946.
(14) Guo, Z.; Manser, J. S.; Wan, Y.; Kamat, P. V.; Huang, L. Spatial and Temporal Imaging of Long-Range Charge Transport in Perovskite Thin Films by Ultrafast Microscopy. *Nat. Commun.* **2015**, *6*, 7471.
(15) Baida, H.; Mongin, D.; Christofilos, D.; Bachelier, G.; Crut, A.; Maioli, P.; Del Fatti, N.; Vallée, F. Ultrafast Nonlinear Optical Response of a Single Gold Nanorod near Its Surface Plasmon Resonance. *Phys. Rev. Lett.* **2011**, *107*, 057402.
(16) Gabriel, M. M.; Kirschbrown, J. R.; Christesen, J. D.; Pinion, C. W.; Zigler, D. F.; Grumstrup, E. M.; Mehl, B. P.; Cating, E. E. M.; Cahoon, J. F.; Papanikolas, J. M. Direct Imaging of Free Carrier and Trap Carrier Motion in Silicon Nanowires by Spatially-Separated Femtosecond Pump−Probe Microscopy. *Nano Lett.* **2013**, *13*, 1336−1340.
(17) Yu, K.; Zijlstra, P.; Sader, J. E.; Xu, Q.-H.; Orrit, M. Damping of Acoustic Vibrations of Immobilized Single Gold Nanorods in Different Environments. *Nano Lett.* **2013**, *13*, 2710−2716.
(18) Huang, L.; Cheng, J.-X. Nonlinear Optical Microscopy of Single Nanostructures. *Annu. Rev. Mater. Res.* **2013**, *43*, 213−236.
(19) Grancini, G.; Polli, D.; Fazzi, D.; Cabanillas-Gonzalez, J.; Cerullo, G.; Lanzani, G. Transient Absorption Imaging of P3HT:PCBM Photovoltaic Blend: Evidence For Interfacial Charge Transfer State. *J. Phys. Chem. Lett.* **2011**, *2*, 1099−1105.
(20) Min, W.; Freudiger, C. W.; Lu, S.; Xie, X. S. Coherent Nonlinear Optical Imaging: Beyond Fluorescence Microscopy. *Annu. Rev. Phys. Chem.* **2011**, *62*, 507−530.
(21) Matthews, T. E.; Piletic, I. R.; Selim, M. A.; Simpson, M. J.; Warren, W. S. Pump-Probe Imaging Differentiates Melanoma from Melanocytic Nevi. *Sci. Transl. Med.* **2011**, *3*, 71ra15.
(22) Moerner, W. E.; Orrit, M. Illuminating Single Molecules in Condensed Matter. *Science* **1999**, *283*, 1670−1676.
(23) Xie, X. S.; Trautman, J. K. Optical Studies of Single Molecules at Room Temperature. *Annu. Rev. Phys. Chem.* **1998**, *49*, 441−480.
(24) Weiss, S. Fluorescence Spectroscopy of Single Biomolecules. *Science* **1999**, *283*, 1676−1683.
(25) Subramanian, S.; Park, S. K.; Parkin, S. R.; Podzorov, V.; Jackson, T. N.; Anthony, J. E. Chromophore Fluorination Enhances Crystallization and Stability of Soluble Anthradithiophene Semiconductors. *J. Am. Chem. Soc.* **2008**, *130*, 2706−2707.
(26) Jurchescu, O. D.; Subramanian, S.; Kline, R. J.; Hudson, S. D.; Anthony, J. E.; Jackson, T. N.; Gundlach, D. J. Organic Single-Crystal Field-Effect Transistors of a Soluble Anthradithiophene. *Chem. Mater.* **2008**, *20*, 6733−6737.
(27) Lee, S. S.; Kim, C. S.; Gomez, E. D.; Purushothaman, B.; Toney, M. F.; Wang, C.; Hexemer, A.; Anthony, J. E.; Loo, Y.-L. Controlling Nucleation and Crystallization in Solution-Processed Organic Semiconductors for Thin-Film Transistors. *Adv. Mater.* **2009**, *21*, 3605−3609.
(28) Jurchescu, O. D.; Mourey, D. A.; Subramanian, S.; Parkin, S. R.; Vogel, B. M.; Anthony, J. E.; Jackson, T. N.; Gundlach, D. J. Effects of Polymorphism on Charge Transport in Organic Semiconductors. *Phys. Rev. B: Condens. Matter Mater. Phys.* **2009**, *80*, 085201.
(29) Li, R.; Ward, J. W.; Smilgies, D.-M.; Payne, M. M.; Anthony, J. E.; Jurchescu, O. D.; Amassian, A. Direct Structural Mapping of Organic Field-Effect Transistors Reveals Bottlenecks to Carrier Transport. *Adv. Mater.* **2012**, *24*, 5553−5558.
(30) Naden, A. B.; Loos, J.; MacLaren, D. A. Structure−function Relations in diF-TES-ADT Blend Organic Field Effect Transistors Studied by Scanning Probe Microscopy. *J. Mater. Chem. C* **2014**, *2*, 245−255.
(31) Anthony, J. E.; Brooks, J. S.; Eaton, D. L.; Parkin, S. R. Functionalized Pentacene: Improved Electronic Properties from Control of Solid-State Order. *J. Am. Chem. Soc.* **2001**, *123*, 9482−9483.
(32) Park, S. K.; Jackson, T. N.; Anthony, J. E.; Mourey, D. A. High Mobility Solution Processed 6,13-Bis(triisopropyl-Silylethynyl) Pentacene Organic Thin Film Transistors. *Appl. Phys. Lett.* **2007**, *91*, 063514.
(33) Sakanoue, T.; Sirringhaus, H. Band-like Temperature Dependence of Mobility in a Solution-Processed Organic Semiconductor. *Nat. Mater.* **2010**, *9*, 736−740.
(34) Diao, Y.; Tee, B. C.-K.; Giri, G.; Xu, J.; Kim, D. H.; Becerril, H. A.; Stoltenberg, R. M.; Lee, T. H.; Xue, G.; Mannsfeld, S. C. B.; et al. Solution Coating of Large-Area Organic Semiconductor Thin Films with Aligned Single-Crystalline Domains. *Nat. Mater.* **2013**, *12*, 665−671.
(35) Walker, B. J.; Musser, A. J.; Beljonne, D.; Friend, R. H. Singlet Exciton Fission in Solution. *Nat. Chem.* **2013**, *5*, 1019−1024.
(36) Mannsfeld, S. C. B.; Tang, M. L.; Bao, Z. Thin Film Structure of Triisopropylsilylethynyl-Functionalized Pentacene and Tetraceno[2,3-B]thiophene from Grazing Incidence X-Ray Diffraction. *Adv. Mater.* **2011**, *23*, 127−131.
(37) Platt, A. D.; Day, J.; Subramanian, S.; Anthony, J. E.; Ostroverkhova, O. Optical, Fluorescent, and (Photo)conductive Properties of High-Performance Functionalized Pentacene and Anthradithiophene Derivatives. *J. Phys. Chem. C* **2009**, *113*, 14006−14014.
(38) Smith, M. B.; Michl, J. Recent Advances in Singlet Fission. *Annu. Rev. Phys. Chem.* **2013**, *64*, 361−386.
(39) Yost, S. R.; Lee, J.; Wilson, M. W. B.; Wu, T.; McMahon, D. P.; Parkhurst, R. R.; Thompson, N. J.; Congreve, D. N.; Rao, A.; Johnson, K.; et al. A Transferable Model for Singlet-Fission Kinetics. *Nat. Chem.* **2014**, *6*, 492−497.
(40) Roberts, S. T.; McAnally, R. E.; Mastron, J. N.; Webber, D. H.; Whited, M. T.; Brutchey, R. L.; Thompson, M. E.; Bradforth, S. E. Efficient Singlet Fission Discovered in a Disordered Acene Film. *J. Am. Chem. Soc.* **2012**, *134*, 6388−6400.
(41) Dillon, R. J.; Piland, G. B.; Bardeen, C. J. Different Rates of Singlet Fission in Monoclinic versus Orthorhombic Crystal Forms of Diphenylhexatriene. *J. Am. Chem. Soc.* **2013**, *135*, 17278−17281.


DOI: 10.1021/acs.jpclett.5b01416
*J. Phys. Chem. Lett.* 2015, 6, 3155−3162

(42) Sharifzadeh, S.; Wong, C. Y.; Wu, H.; Cotts, B. L.; Kronik, L.; Ginsberg, N. S.; Neaton, J. B. Relating the Physical Structure and Optoelectronic Function of Crystalline TIPS-Pentacene. *Adv. Funct. Mater.* **2015**, *25*, 2038−2046.
(43) James, D. T.; Frost, J. M.; Wade, J.; Nelson, J.; Kim, J.-S. Controlling Microstructure of Pentacene Derivatives by Solution Processing: Impact of Structural Anisotropy on Optoelectronic Properties. *ACS Nano* **2013**, *7*, 7983−7991.
(44) Bräuer, B.; Virkar, A.; Mannsfeld, S. C. B.; Bernstein, D. P.; Kukreja, R.; Chou, K. W.; Tyliszczak, T.; Bao, Z.; Acremann, Y. X-Ray Microscopy Imaging of the Grain Orientation in a Pentacene Field-Effect Transistor. *Chem. Mater.* **2010**, *22*, 3693−3697.
(45) Schuettfort, T.; Watts, B.; Thomsen, L.; Lee, M.; Sirringhaus, H.; McNeill, C. R. Microstructure of Polycrystalline PBTTT Films: Domain Mapping and Structure Formation. *ACS Nano* **2012**, *6*, 1849−1864.
(46) Kowarik, S.; Broch, K.; Hinderhofer, A.; Schwartzberg, A.; Ossó, J. O.; Kilcoyne, D.; Schreiber, F.; Leone, S. R. Crystal Grain Orientation in Organic Homo- and Heteroepitaxy of Pentacene and Perfluoropentacene Studied with X-Ray Spectromicroscopy. *J. Phys. Chem. C* **2010**, *114*, 13061−13067.
(47) Lee, S. S.; Loth, M. A.; Anthony, J. E.; Loo, Y.-L. Orientation-Independent Charge Transport in Single Spherulites from Solution-Processed Organic Semiconductors. *J. Am. Chem. Soc.* **2012**, *134*, 5436−5439.
(48) Hiszpanski, A. M.; Loo, Y.-L. Directing the Film Structure of Organic Semiconductors via Post-Deposition Processing for Transistor and Solar Cell Applications. *Energy Environ. Sci.* **2014**, *7*, 592−608.



DOI: 10.1021/acs.jpclett.5b01416
*J. Phys. Chem. Lett.* 2015, 6, 3155−3162